

16. L. W. Braille, W. J. Hinze, G. R. Keller, E. G. Lidiak, J. L. Sexton, *Tectonophysics* **131**, 1 (1986).
17. M. D. Zoback et al., *Science* **209**, 971 (1980).
18. R. T. Cox and R. B. Van Arsdale, *Eng. Geol.* **46**, 210 (1997).
19. C. A. Swanberg and P. Morgan, in *Physical Properties of Rocks and Minerals*, Y. S. Touloukian, W. R. Judd, R. F. Roy, Eds. (McGraw-Hill, New York, 1981), vol. 2, pp. 540-548; C. A. Swanberg, B. J. Mitchell, R. L. Lohse, D. D. Blackwell, in *Investigations of the New Madrid, Missouri, Earthquake Region*, F. A. McKeown and L. C. Pakiser, Eds., *U.S. Geol. Surv. Prof. Pap.* **1236** (1982), pp. 185-189.
20. A. Ginzburg, W. D. Mooney, A. W. Walter, W. J. Lutter, J. H. Healy, *Am. Assoc. Pet. Geol. Bull.* **67**, 2031 (1983); W. D. Mooney, M. C. Andrews, A. Ginzburg, D. A. Peters, R. M. Hamilton, *Tectonophysics* **94**, 327 (1983).
21. An alternative explanation for lower crustal weakness is proposed by M. F. Kane [in *Studies Related to the Charleston, South Carolina, Earthquake of 1886: A Preliminary Report*, D. W. Rankin, Ed., *U.S. Geol. Surv. Prof. Pap.* **1028-O** (1977), pp. 199-204]. A weak crust is hypothesized to exist by (5), (13), (18), and F. A. McKeown and S. F. Diehl [in *Investigations of the New Madrid Seismic Zone*, K. M. Shedlock and A. C. Johnston, Eds., *U.S. Geol. Surv. Prof. Pap.*, **1538-N** (1994), pp. 1-24].
22. *ABAQUS User's Manual, version 5.8* [Hibbit, Karlsson & Sorensen, Inc., Pawtucket, RI (1998)]. Variably sized (minimum 0.2 km by 0.5 km by 0.25 km) brick elements are used. Variations in total number of elements (69%) and number of elements along the fault plane (53%) change the average recurrence interval for  $M > 7.0$  events by ~100 years. A symmetry condition is applied along a plane oriented perpendicular to the fault at its midpoint (Fig. 2).
23. Maxwell viscoelastic materials have no long-term elastic stiffness. The weak zone could more reasonably be defined to have some long-term stiffness. Unless the stress relaxed by the weakening zone becomes too small to trigger fault slip, the fundamental behavior of the model would not change.
24. The shear stress failure criteria is evaluated at each node on the seismogenic fault plane (defined using contact surfaces) at each time increment. During any increment, nodes can fail either independently or in groups. For failure initiation, the maximum resolved stress must be within 1.6% of  $\tau^{\max}$  (time step is adjusted to meet this criteria). Multiple nodes cannot fail simultaneously unless the time step is  $\leq 10$  years. Variations in these criteria by a factor of 2 change the average recurrence interval for  $M > 7.0$  events by ~50 years.
25. Stresses measured in deep boreholes [J. Townend and M. D. Zoback, *Geology* **28**, 399 (2000)] and shallow stress measurements from the NMSZ region [W. L. Ellis, in *Investigations of the New Madrid Seismic Zone*, K. M. Shedlock and A. C. Johnston, Eds., *U.S. Geol. Surv. Prof. Pap.* **1538-B** (1994), pp. 1-13] are comparable.
26. For a Voigt solid with viscous element representing the lower crustal weak zone and elastic element representing the upper crust, the time for a fraction  $P$  of the total strain to accumulate following imposition of a fixed stress is  $T_{\text{total}} = -\ln(1 - P)/(\eta_w/\mu)$  where  $P = 0.99$ ,  $T_{\text{total}} = 10,000$  years, and  $\mu = 3.5 \times 10^4$  MPa yields  $\eta_w = 2.4 \times 10^{21}$  Pa-s. Because postseismic stress cycling between the upper and lower crust is not included in this approximation, numerical models require lower viscosities to obtain comparable characteristic relaxation times.
27. We estimate earthquake recurrence interval by the earthquake stress drop divided by the fault stressing rate. For a Maxwell layer of thickness  $h_2$  underlying an elastic layer of thickness  $h_1$ , stressing rate is given by  $\tau^{\dot{}}(h_2\mu/h_1\eta_w)\exp(-h_1\mu t/h_1\eta_w)$ , where  $h = (h_2 + h_1)$  (35) and  $t$  is time since the initiation of relaxation. The recurrence interval is given by  $(\tau^{\max} - \tau^{\text{residual}})/\tau^{\dot{}}(h_1\mu/h_2\mu)\exp(h_1\mu t/h_1\eta_w)$ .
28. W. Thatcher, in *The San Andreas Fault System, California*, R. E. Wallace, Ed., *U.S. Geol. Surv. Prof. Pap.* **1515** (1990), pp. 189-205.
29. T. J. Hughes et al., in *The Last Great Ice Sheets*, G. H. Denton and T. J. Hughes, Eds. (Wiley, New York, 1981), pp. 275-318; P. A. Mayewski, G. H. Denton, T. J. Hughes, in *The Last Great Ice Sheets*, G. H. Denton and T. J. Hughes, Eds. (Wiley, New York, 1981), pp. 67-178; H. S. Hasegawa and P. W. Basham, in *Earthquakes at North Atlantic Passive Margins: Neotectonics and Postglacial Rebound*, S. Gregersen and P. W. Basham, Eds. (Kluwer, Boston, 1989), pp. 483-500; A. C. Johnston, in *Earthquakes at North Atlantic Passive Margins: Neotectonics and Postglacial Rebound*, S. Gregersen and P. W. Basham, Eds. (Kluwer, Boston, 1989), pp. 581-599.
30. B. Grollmund and M. D. Zoback [Geology, in preparation] suggest the possibility of glacial triggering in an anomalously weak NMSZ. Using a laterally homogeneous model, P. Wu and P. Johnston [*Geophys. Res. Lett.* **27**, 1323 (2000)] find that glacial triggering is unlikely.
31. R. T. Saucier, *Geomorphology and Quaternary Geologic History of the Lower Mississippi Valley* (U.S. Army Corps of Engineers, Mississippi River Commission, Vicksburg, MS, 1994), vol. 1, 362 pp., vol. 2, 28 plates.
32. J. Langbein and H. Johnson, *J. Geophys. Res.* **102**, 591 (1997).
33. We use an actual GPS covariance matrix from the NMSZ, representing the scaled weighted mean of daily solutions taken over a 2-week period in 1997. Horizontal uncertainties are ~3 mm.
34. We use a Kalman filtering approach following P. Segall and M. Matthews [*J. Geophys. Res.* **102**, 22391 (1997)] in which the data is assumed to result from a combination of uniform strain plus random benchmark motion and measurement error. We assume that the scale of the random walk process is known. Additional error would result if this parameter must be estimated directly from the data.
35. N. J. Kusznir and M. H. P. Bott, *Tectonophysics* **43**, 247 (1977).
36. We thank M. H. Murray for help with the GPS uncertainty analysis and B. Grollmund and M. D. Zoback for their insights regarding the NMSZ and glacial triggering.

25 May 2000; accepted 20 July 2000

## Dating of Pore Waters with <sup>129</sup>I: Relevance for the Origin of Marine Gas Hydrates

Udo Fehn,<sup>1\*</sup> Glen Snyder,<sup>1</sup> Per K. Egeberg<sup>2</sup>

Pore waters associated with gas hydrates at Blake Ridge in the Atlantic Ocean were dated by measuring their iodine-129/iodine ratios. Samples collected from sediments with ages between 1.8 and 6 million years ago consistently yield ages around 55 million years ago. These ages, together with the strong iodine enrichment observed in the pore waters, suggest that the origin of iodine is related to organic material of early Tertiary age, which probably is also the source of the methane in the gas hydrates at this location.

Gas hydrates are a potentially large source of energy and of greenhouse gases (1). Recent surveys suggest that they are ubiquitous features of continental slopes and that the energy equivalent of the methane in hydrates could potentially surpass that of all the known reservoirs of crude oil and natural gas combined. Marine gas hydrates commonly consist of methane trapped in a lattice of water ice (2) and are found in a specific depth range in marine sediments, typically between 200 and 500 m below the seafloor (mbsf). On seismic profiles, the bottom of the gas hydrate zone is indicated by a strong reflector, the bottom-simulating reflector (BSR). Below the BSR, free methane gas is common; its concentration is, however, considerably lower than the methane bound as gas hydrates.

The origin and formation of gas hydrates have been the focus of a growing number of studies (1-3). Although it is generally assumed that gas hydrates are related to the

deposition and subsequent diagenesis of organic matter in marine sediments, no consensus exists on whether the methane in the hydrates formed at their present location or migrated from different source areas. To address this question, we used the <sup>129</sup>I system to date the origin of these hydrocarbons.

The cosmogenic radioisotope <sup>129</sup>I (half-life of 15.7 million years) is produced by the spallation of Xe isotopes in the atmosphere and by spontaneous fission of <sup>238</sup>U in the crust. Both of these mechanisms contribute similar amounts of natural <sup>129</sup>I to surface reservoirs (4). Iodine moves quickly through most surface reservoirs and is considered isotopically homogeneous at the surface of Earth, including the oceans and shallow sediments. The isotopic equilibrium of I in surface reservoirs has been disturbed recently by releases from weapons tests and reprocessing plants, which have increased the concentrations of <sup>129</sup>I in fresh waters, soils, surface ocean water, and shallow sediments by several orders of magnitude (5-8).

Iodine has one stable isotope, <sup>127</sup>I, and its isotopic composition is reported as <sup>129</sup>I/I. Recent sediments without anthropogenic I have <sup>129</sup>I/I of  $1.5 \times 10^{-12}$  (5, 9). This ratio, which is used as a starting value for <sup>129</sup>I-

<sup>1</sup>Department of Earth and Environmental Sciences, University of Rochester, Rochester, NY 14627, USA.

<sup>2</sup>Department of Chemistry, Agder College, Tordenskjoldgate 65, 4604 Kristiansand, Norway.

\*To whom correspondence should be addressed. E-mail: fehn@earth.rochester.edu

REPORTS

based age calculations, is more than two orders of magnitude above the detection limit of accelerator mass spectrometry (AMS), the method of choice for the detection of cosmogenic radioisotopes. Although the generally low concentrations of iodine in many environments often make it difficult to collect enough sample material, the very high concentrations of iodide found in the pore waters at Blake Ridge (10) allowed the preparation of an AMS sample from the 3 to 5 ml collected from the sediment cores. The half-life of  $^{129}\text{I}$ , together with the observed input ratios and the detection limit for  $^{129}\text{I}/\text{I}$ , allows applications of this dating method within a range of about 80 million years ago (Ma). The biophilic nature of iodine suggests that this isotopic system is particularly useful for the dating and tracing of organic material (11–15).

The samples used in this study were collected during Leg 164 of the Ocean Drilling Program (ODP) from Site 997 on Blake Ridge. Blake Ridge is a large drift deposit

that extends about 400 km in a southeast direction from the continental rise of the passive margin of the southeastern United States. The top of the ridge is at depths of 2500 to 3000 m (Fig. 1). The sedimentary package in this area is up to 10 km thick, consisting of sediments deposited continuously from the Jurassic to the present (16). The presence of gas hydrates at Blake Ridge is identified by an essentially continuous BSR at depths of 450 to 500 mbsf. The upper boundary of the hydrate layer is not as well defined, with estimates varying between 240 mbsf (17) and 24 mbsf (10, 18). Free methane is found below the BSR, with dissociation of gas hydrates occurring above the gas hydrate layer. Core recovery from this site was excellent, and pore waters were collected from 0 to 750 mbsf, covering the full range of gas hydrate occurrence.

For this study, we selected seven samples from the collection of pore water samples from ODP Site 997 (Table 1) (19). The pore water samples had between 3 and 5 ml of

fluid with iodide concentrations between 1.19 and 1.72 mM. The lowest concentration was found in the top sample, whereas concentrations in the other six samples fell into a quite narrow range between 1.5 and 1.72 mM. The pore waters show a marked increase in iodide concentrations from levels below 0.001 mM close to the sediment-water interface to values up to 1.5 mM at depths below 100 mbsf. This strong increase in iodide levels is accompanied by a parallel increase in bromide concentrations and is in contrast to the behavior of chloride concentrations, which decrease from a surface value of 560 mM to values close to 520 mM throughout the interval with some variations in the area occupied by gas hydrates (Fig. 2). These values can be compared with seawater concentrations of 533 mM for chloride, 0.839 mM for bromide, and 0.00045 mM for total dissolved iodine (20). Although chloride concentrations in these sediments are close to seawater concentrations, iodide in these pore waters is enriched by more than three orders of magnitude and bromide by a factor of 4. Comparison with seawater concentrations indicates that the main source of chloride is probably connate seawater but that iodide (and bromide to a lesser degree) must have an additional source in order to explain the observed strong enrichment. Given the biophilic character of iodine, it is likely that the enrichment reflects the release of iodide from the decomposition of organic matter in marine sediments (21) and is thus directly related to the origin of the gas hydrates. Bromide enrichment is also commonly related to the release from organic sources. A good correlation ex-

Fig. 1. Location map of Blake Ridge with ODP Site 997 and the USGS line 32. Shaded area indicates the occurrence of gas hydrates, based on the presence of a BSR. Water depth at Site 997 was 2770 m; the BSR was penetrated at 451 mbsf.

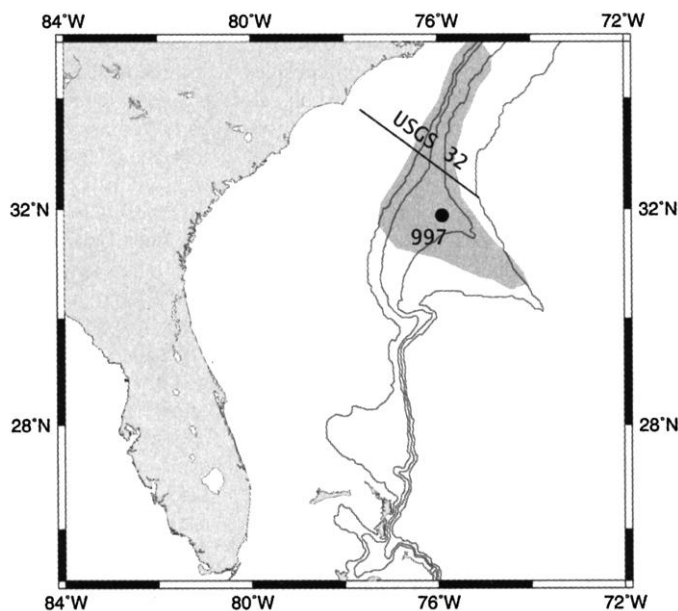


Table 1. Concentrations, isotope ratios, and ages of pore waters. Concentrations have  $1\sigma$  uncertainties of 3.3% ( $\text{Cl}^-$ ), 2.3% ( $\text{Br}^-$ ), and 0.48% ( $\text{I}^-$ ). Sed. age, depositional age of sediments containing hydrates; fluid age, sediment age corrected for expulsion of pore waters because of compaction; min. age, age based on decay of initial ratio of  $^{129}\text{I}/\text{I} = 1500 \times 10^{-15}$ ; corr. age, age corrected for in situ buildup of  $^{129}\text{I}$  in deep sediments.

Sample	Depth (mbsf)	$\text{Cl}^-$ (mM)	$\text{Br}^-$ (mM)	$\text{I}^-$ (mM)	U (ppm)	$^{129}\text{I}/\text{I}$ ( $\times 10^{-15}$ )	Sed. age (Ma)	Fluid age (Ma)	Min. age (Ma)	Corr. age (Ma)
997A35X	275.2	471	2.59	1.19	2.7	$220 \pm 60$	1.8	4.65	$43.6 \pm 7.3$	48.8
997A46X	367.15	500	2.91	1.49	3.44	$155 \pm 20$	2.6	5.98	$51.6 \pm 3.3$	58.2
997A52X	411.25	491	2.97	1.53	3.31	$181 \pm 32$	2.95	6.58	$48.1 \pm 4.6$	53.3
997B14X	493.56	515	3.23	1.72	2.69	$127 \pm 54$	3.63	7.68	$56.1 \pm 12.8$	63.3
997B24X	572.25	519	3.13	1.70	2.67	$125 \pm 19$	4.35	9.76	$56.5 \pm 3.9$	63.8
997B33X	642.72	516	3.05	1.63	2.15	$142 \pm 29$	5.01	9.68	$53.6 \pm 5.4$	60.1
997B39X	687.65	514	3.04	1.66	2.43	$214 \pm 32$	5.46	10.3	$44.3 \pm 3.8$	48.0

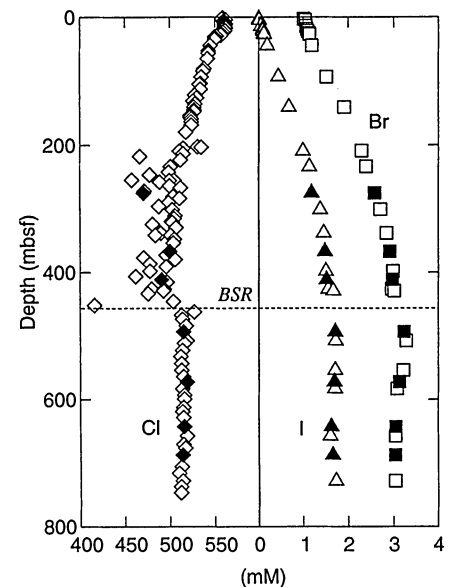


Fig. 2. Concentration profiles for chloride (diamonds), bromide (squares), and iodide (triangles) at Site 997. Solid symbols indicate the samples used for the  $^{129}\text{I}/\text{I}$  determinations.

ists between  $\text{Cl}^-$  concentrations and  $\text{I}^-$  and  $\text{Br}^-$  concentrations (Fig. 3). The concentrations of  $\text{Br}^-$  and  $\text{I}^-$  in these pore waters are much higher than in seawater, in contrast to the  $\text{Cl}^-$  values, which essentially reflect seawater concentrations, diluted perhaps by low-chlorinity water advected from below (18) or by the dissociation of gas hydrates.

Iodine extracted from the pore water samples was used to prepare samples for the determination of  $^{129}\text{I}/\text{I}$  ratios by AMS (22). All the  $^{129}\text{I}/\text{I}$  values are considerably below the value for recent marine sediments ( $1.5 \times 10^{-12}$ ), indicating that old iodine is indeed present in these samples. With the use of this ratio as the input ratio for marine iodine, ages can be calculated on the basis of the decay constant of  $^{129}\text{I}$  ( $4.4 \times 10^{-8} \text{ year}^{-1}$ ). Except for the deepest and most shallow samples, all the ages are close to 50 Ma; the other two ages are lower by about 5 Ma.

The ages found for the pore waters need to be put into the context of the depositional environment. Figure 4 compares the iodine ages with the ages determined for the deposition of the sediments in Site 997, which cover a range between 1.8 and 5.5 Ma. During the deposition of sediments and subsequent compaction, waters are squeezed out and forced into the new, additional layers on top. Therefore, pore waters are considered to be older than the age of the associated sediments. The difference between these ages has been modeled by assuming constant rate of deposition and no migration of pore waters (23). Even considering this correction (Fig. 4), iodine ages indicate that iodine was not deposited together with these sediments and

had to have migrated into the sediments sometime after their deposition.

Two potential corrections for the iodine ages need to be considered, correction for the addition of in situ-produced  $^{129}\text{I}$  and for the introduction of anthropogenic  $^{129}\text{I}$ . Because both of these processes would have added  $^{129}\text{I}$  to the pore waters, the calculated iodine ages are minimum values. The element distribution found for the pore water samples makes contamination by surface components highly unlikely, so that correction for anthropogenic  $^{129}\text{I}$  does not seem necessary here. The addition of in situ-produced  $^{129}\text{I}$  could have occurred either in the source formations or in the sediments where it was found, the reservoir formations. Time-dependent in situ addition is mainly a function of the concentration of uranium and the escape probability of the fissiogenic  $^{129}\text{I}$  (24).

If it came from the reservoir formations, the amount of  $^{129}\text{I}$  added can be calculated with the observed uranium concentrations, porosities, and the ages of the formations. If we assume that all the  $^{129}\text{I}$  produced by the spontaneous fission of  $^{238}\text{U}$  in the reservoir sediments has found its way into the pore waters, an upper limit for this correction results. Uranium concentrations in these sediments are between 2 and 3 parts per million (ppm), with porosities around 50%. Given these figures, we can calculate additions both for sediment ages (between 1.8 and 5.5 Ma) and pore water ages (between 4.6 and 10.3 Ma). The maximum correction based on these assumptions is a lowering by  $12 \times 10^{-15}$  of the ratio for the deepest sample. Because this change in ratio corresponds to an increase in age of only slightly more than 1 Ma, it is well within the error limits of the determinations and therefore will be ignored in further discussion.

A larger correction could be made on the basis of the residence time of the pore waters in deeper layers. Because these fluids must have resided somewhere in the sediment pile

for the time determined before, it is quite likely that fissiogenic  $^{129}\text{I}$  has been added during that time. Although the specific location of residence for these waters is not known, uranium concentrations and porosity values probably were not markedly different from the values found in the shallow sediments. As a first approximation, we can therefore apply the same approach as before, using, however, 3 ppm of uranium and the ages determined by the  $^{129}\text{I}/\text{I}$  ratios. Because longer times are involved in this calculation, the corrections are more substantial than those determined for the shallow sediments. The average age of the pore waters increases from 50.5 to 56.5 Ma; individual corrected ages are also listed in Table 1. Because in all these cases we assumed that all of the fissiogenic  $^{129}\text{I}$  escaped from the sediments into the pore waters, the results of these calculations are probably too high. Although corrections for in situ production can be substantial, they do not change the overall range of results, nor do they seem to influence the differences between the individual results.

The most striking result of these determinations is that all the ages for the pore waters are consistently and substantially older than the age of the host sediments. The ages indicate that the source of iodine in the pore waters is from the early Tertiary. According to a cross section of this area [U.S. Geological Survey (USGS) line 32], sediments of this age are present in this area, generally between 1 and 3 km below the sea floor (16). Although the ages determined here reflect strictly only the origin of the iodine in the pore waters, it seems reasonable to assume that iodine migrated together with the fluids into their current positions. Given the geochemical behavior of iodine, the most likely cause for the observed strong enrichment is the release of iodine during the diagenesis of organic material of early Tertiary age. A large amount of organic material is needed to explain the enrichment of the waters by factors of more than 4000 over the typical concentrations in seawater. This organic material likely was also the origin of the methane found together with the pore waters in the form of gas hydrates. This suggests that the organic parent material of the gas hydrates is of early Tertiary age and that gases and waters migrated together to their current positions from depths between 1 and 3 km below the sea floor.

Iodide concentrations are not routinely measured in pore waters, so it is not known to what extent the observed correlation between high iodide concentrations and hydrate occurrence is representative. If such a correlation is common, the  $^{129}\text{I}$  method could be used on a broad scale to determine the age of the sources of gas hydrates. The age found for this deposit, close to 55 Ma, is one in which large depositions of marine organic material have been observed, perhaps associated with a large-scale change in

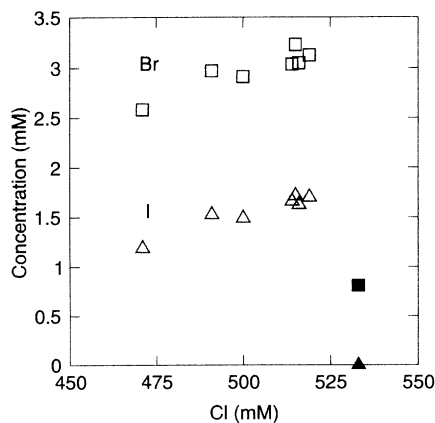


**Fig. 3.** Br (squares) and I (triangles) concentrations increase linearly with Cl concentration. Pore fluids have Cl concentrations close to but slightly lower than seawater [solid square, marine Br; solid triangle, marine I, plotted at Cl seawater concentrations (20)] but are enriched in Br by a factor of 4 and in I by a factor of 4000. Although the degree of enrichment is very different, the close correlation between Br and I concentrations in the pore fluids suggests a common diagenetic source as cause for the enrichment.

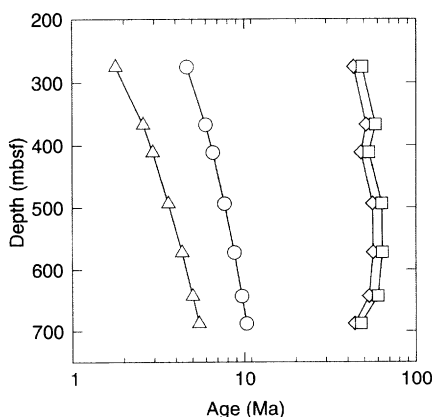


**Fig. 4.** Age-depth profile for sediments (triangles), sediment pore fluids after correction for compaction (circles), minimum iodine ages (diamonds), and iodine ages corrected for in situ production of  $^{129}\text{I}$  from uranium (squares).

oceanic circulation (25). Source ages determined with the <sup>129</sup>I system in the Gulf Coast region (12) are also close to those of this study. If iodine ages determined in pore fluids associated with other gas hydrate deposits fall into the same time range, the case would be strengthened that the period around 55 Ma was responsible for large-scale deposition of organic matter and subsequent hydrocarbon generation in the oceans.

References and Notes

1. K. A. Kvenvolden, *Proc. Natl. Acad. Sci. U.S.A.* **96**, 3420 (1999).
2. E. D. Sloan, *Clathrate Hydrates of Natural Gases* (Decker, New York, 1990).
3. W. Y. Xu and C. Ruppel, *J. Geophys. Res.* **104**, 5081 (1999).
4. J. T. Fabryka-Martin, H. Bentley, D. Elmore, P. L. Airey, *Geochim. Cosmochim. Acta* **49**, 337 (1985).
5. U. Fehn et al., *Geophys. Res. Lett.* **13**, 137 (1986).
6. D. R. Schink, P. H. Santschi, O. Corapcioglu, P. Sharma, U. Fehn, *Earth Planet. Sci. Lett.* **135**, 131 (1995).
7. U. Rao and U. Fehn, *Geochim. Cosmochim. Acta* **63**, 1927 (1999).
8. U. Fehn and G. Snyder, *Nucl. Instrum. Methods*, in press.
9. J. E. Moran, U. Fehn, R. T. D. Teng, *Chem. Geol.* **152**, 193 (1998).
10. P. K. Egeberg and G. R. Dickens, *Chem. Geol.* **153**, 53 (1999).
11. U. Fehn et al., *Geochim. Cosmochim. Acta* **56**, 2069 (1992).
12. J. E. Moran, U. Fehn, J. S. Hanor, *Geochim. Cosmochim. Acta* **59**, 5055 (1995).
13. W. C. Riese, S. G. Franks, U. Fehn, J. E. Moran, *Am. Assoc. Pet. Geol.* **1999**, A116 (1999).
14. G. T. Snyder and U. Fehn, *Nucl. Instrum. Methods*, in press.
15. G. T. Snyder, U. Fehn, F. Goff, *Eos (West Pac. Geophys. Meet. Suppl.)* **81**, 178 (2000).
16. D. R. Hutchison et al., *AAPG Mem.* **34**, 129 (1982).
17. R. Matsumoto and W. S. Borowski, *Proc. Ocean Drill. Program. Sci. Results* **164**, 59 (2000).
18. R. Hesse, S. K. Frape, P. K. Egeberg, R. Matsumoto, *Proc. Ocean Drill. Program Sci. Results* **164**, 129 (2000).
19. The pore water samples were squeezed from the sediments at shipboard following standard procedures and immediately sealed in glass bottles. Chloride was determined on shipboard by argentometric titration, and iodide and bromide concentrations were determined by the iodometric method and spectrophotometry (10).
20. Geochemical Earth Reference Model (2000), <http://earthref.org/GERM/>.
21. J. B. Martin, J. M. Gieskes, M. Torres, M. Kastner, *Geochim. Cosmochim. Acta* **57**, 4377 (1993).
22. Iodine was extracted from the samples and precipitated as AgI, with standard procedures (17). About 1 mg of iodine is needed to produce a reliable <sup>129</sup>I/I ratio with AMS. The samples yielded between 1 and 2 mg of AgI each, which was used for the isotope determination at the PrimeLab AMS system, Purdue University (26). As usual for isotopic dating systems, uncertainty in input ratio and the decay constant were not considered in the age calculations.
23. Determination of sediment and pore water age: Assume a constant rate of sediment deposition and steady state porosity profile  $P(x) = (P_0 - P_{inf})\exp(-Lx) + P_{inf}$ . Derive expression for sediment age:  $F_w(x)$  (flux of sediment in kg m<sup>-2</sup> year<sup>-1</sup>) =  $W(x) * R_s * S(x) = s$  (constant because of steady state) =>  $W(x) = (s/R_s)S(x)^{-1}$  (m year<sup>-1</sup>). The age of sediment particles  $S_{age}(x)$  is

$$S_{age}(x) = \int_0^x W(x)^{-1} dx$$

Derive the expression for pore water age:  $F_w$  (flux of pore water in kg m<sup>-2</sup> year<sup>-1</sup>) =  $V(x)R_wP(x)$  => con-

stant (because of steady state). The constant is derived by the argument that at the depth of fully compacted sediment ( $x_{inf}$ ), particles and pore water are buried at the same rate =>  $V_{inf} = W_{inf}$ . Hence,  $F_w = W_{inf}R_wP_{inf} = V(x)R_wP(x)$  =>  $V(x) = W_{inf}P_{inf}/P(x)$ . The age of pore water  $P_{age}(x)$  is

$$P_{age}(x) = \int_0^x V(x)^{-1} dx$$

The variables are as follows:  $P_0$ , porosity at sediment surface (0.72);  $P_{inf}$ , porosity at "fully compacted" sediment (0.43);  $L = 0.002$ ;  $R_w$ , density of pore water (1000 kg m<sup>-3</sup>);  $R_s$ , density of particles (2500 kg m<sup>-3</sup>);  $s$ , rate of particle deposition at sediment surface (0.130 kg m<sup>-2</sup> year<sup>-1</sup>);  $P(x)$ , porosity profile;  $S(x) = 1 - P(x)$ , "sedimentosity" profile;  $V(x)$ , rate of pore water flow relative to sediment surface (m year<sup>-1</sup>); and  $W(x)$ , rate of particle burial relative to sediment surface (m year<sup>-1</sup>). Boundary conditions for sediment ages are derived from biostratigraphic data for Blake Ridge (27).

24. The addition of fissionogenic <sup>129</sup>I is described in the following equation:

$$N_{129} = (N_{238}Y_{st}\lambda_{st}\rho_s)(E/P)[1 - \exp(-\lambda_{129}t)]/\lambda_{129}$$

where  $N_{129}$  is the concentration of fissionogenic <sup>129</sup>I in the pore waters,  $N_{238}$  is the concentration of <sup>238</sup>U in the sediments,  $Y_{st}\lambda_{st}$  is the product of the yield and the decay constant for spontaneous fission at mass 129,  $\rho_s$  is the density of sediments,  $E/P$  is the ratio of the escape efficiency to the effective porosity of the sediments,  $\lambda_{129}$  is the decay constant for <sup>129</sup>I, and  $t$  is the residence time of the pore water in the sediments. The following values were used for this calculation [see (17) for source references]:  $\lambda_{st} = 8.5 \times 10^{-17}$  year<sup>-1</sup>;  $Y_{st} = 0.0003$ ;  $\rho_s = 2.4$  kg/l;  $E/P = 2$ ; and  $\lambda_{129} = 4.4 \times 10^{-8}$  year<sup>-1</sup>.

25. G. R. Dickens, M. M. Castillo, J. C. G. Walker, *Geology* **25**, 259 (1997).
26. D. Elmore et al., *Nucl. Instrum. Methods* **123**, 69 (1997).
27. H. Okada, *Proc. Ocean Drill. Program Sci. Results* **164**, 331 (2000).
28. We thank D. Elmore and P. Sharma for the <sup>129</sup>I/I determinations and J. Gieskes and R. Hesse for helpful comments. U.F. acknowledges the hospitality provided by the Beppu Geothermal Institute, Kyoto University, which allowed the timely completion of this report. The research was supported in part by NSF grant OCE-9907024 to U.F.

1 May 2000; accepted 20 July 2000

# Polyploidy and the Evolution of Gender Dimorphism in Plants

J. S. Miller\* and D. L. Venable

Gender dimorphism and polyploidy are important evolutionary transitions that have evolved repeatedly in many plant families. We show that gender dimorphism in North American *Lycium* (Solanaceae) has evolved in polyploid, self-compatible taxa whose closest relatives are cosexual, self-incompatible diploids. This has occurred independently in South African *Lycium*. We present additional evidence for this pathway to gender dimorphism from 12 genera involving at least 20 independent evolutionary events. We propose that polyploidy is a trigger of unrecognized importance for the evolution of gender dimorphism, which operates by disrupting self-incompatibility and leading to inbreeding depression. Subsequently, male sterile mutants invade and increase because they are unable to inbreed.

The evolution of sex and sexual systems is a central issue of evolutionary biology, and the deployment of sexual function into one or more morphs is a core concern (1, 2). Gender dimorphism (the presence of two sexual morphs in a population) occurs in only ~10% of angiosperm species but has evolved from cosexual ancestors in nearly half of the angiosperm families, making it an important evolutionary trend (3). Several pathways for the evolution of gender dimorphism have been advanced (3–5). The mechanistic explanations for the transition from cosexuality to gender dimorphism have concentrated on overcoming the inherent 50% fitness loss of single-sexed nuclear gene mutants arising in cosexual populations (6, 7). These mechanisms fall into two broad nonexclusive categories: elimination of inbreeding depression

(IBD) by male sterile mutants (i.e., selection for outcrossing) and compensatory resource reallocation following the loss of one sexual function. Whereas both factors are thought to be important in the evolution of gender dimorphism, the outcrossing scenarios have more empirical support and are widely advanced as the principal mechanism favoring gender dimorphism (8). Because inbreeding avoidance is not important for self-incompatible taxa, the prominence accorded the inbreeding avoidance mechanism has led to a search for a correlation between the occurrence of separate sexes and an evolutionary background of self-compatibility (9, 10).

Polyploidy disrupts self-incompatibility in many species (11, 12). The tendency for polyploids to express self-compatibility [due to genetic interactions in diploid pollen grains (13)] allows for the establishment of otherwise reproductively isolated polyploids (11, 14). Because polyploids buffer the effects of selfing more effectively than diploids (11, 15, 16), the resultant polyploid plants may be shielded initially

Department of Ecology and Evolutionary Biology, University of Arizona, Tucson, AZ 85721, USA.

\*To whom correspondence should be addressed. E-mail: jsmiller@email.arizona.edu